Chapter 7

A robust numerical scheme for two-parameter singularly perturbed parabolic problems with a discontinuous convection term coefficient and source term

7.1 Introduction

In this chapter, a numerical scheme is constructed for the problems in which the diffusion and convection parameters (ε_1 and ε_2, respectively) both are small, and the convection term coefficient and source terms have a jump discontinuity in the domain of consideration. Two different cases depending on the magnitude of the ratios $\varepsilon_1/\varepsilon_2^2$, and $\varepsilon_2^2/\varepsilon_1$ have been considered separately. Through rigorous analysis, the theoretical error bounds on the singular and regular components of the solution are obtained separately, which shows that in both cases the method is convergent uniformly irrespective of the size of the parameters $\varepsilon_1, \varepsilon_2$. Test problems are included to validate the theoretical results.

Define $\Omega^- = (0,e), \Omega^+ = (e,1), \Omega^e = \Omega^- \cup \Omega^+, \Omega = (0,1), \Lambda = (0,T], D^- = \Omega^- \times \Lambda, D^+ = \Omega^+ \times \Lambda, D^e = D^- \cup D^+, D = \Omega \times \Lambda$, where T is a fixed real number. We consider the following two-parameter singularly perturbed boundary value problem (SP-BVP)

$$L\psi(x,t) \equiv -\psi_t + \varepsilon_1 \psi_{xx} + \varepsilon_2 a(x,t)\psi_x - b(x,t)\psi = f(x,t), \quad (x,t) \in D^e, \tag{7.1a}$$

$$\psi(0,t) = \psi_l(t) \text{ on } \Upsilon_l, \quad \psi(1,t) = \psi_r(t) \text{ on } \Upsilon_r, \tag{7.1b}$$

$$\psi(x,0) = \psi_b(x) \text{ on } \Upsilon_b, \tag{7.1c}$$

where $0 < \varepsilon_1, \varepsilon_2 \ll 1$ are the diffusion and convection parameters respectively. $\Upsilon = \Upsilon_l \cup \Upsilon_b \cup \Upsilon_r$, where $\Upsilon_l = \{(x,t) : \ x = 0, t \in \overline{\Lambda}\}$, $\Upsilon_b = \{(x,t) : \ t = 0, x \in \overline{\Omega}\}$, and $\Upsilon_r = \{(x,t) : \ x = 1, t \in \overline{\Lambda}\}$ is a part of the boundary of D. We assume that $a(x,t)$ and $f(x,t)$ are sufficiently smooth in D except the jump discontinuity at $e \in \Omega$ denoted by $[w](e) = w(e^+) - w(e^-)$. Furthermore, we assume

(A1) $a(x,t) \leq -\kappa_1 < 0$ in D^- and $a(x,t) \geq \kappa_2 > 0$ in D^+.

(A2) The functions $b(x,t)$ (in $\overline{D}$), and $\psi_l(t)$, $\psi_r(t)$, $\psi_b(x)$ (on Υ) are bounded and sufficiently smooth.

(A3) $b(x,t) \geq \beta^* > 0$ in $\overline{D}$.

(A4) The initial function satisfies the compatibility conditions.

The uniqueness of the solution of the problem (7.1) is confirmed by (A1)-(A4). In general, the small diffusion parameter leads to the twin boundary layers and the discontinuity in the convection term coefficient and source terms lead to an interior layer in the solution. Moreover, in general, the layer behaviour is determined by the magnitude of the ratios of the diffusion parameter to the square of the convection parameter, and the fact whether the convection-coefficient $a(x,t)$ is negative or positive. In particular, the boundary layers widths depend continuously on these ratios, and the interior layer occurs at both sides of the point of the discontinuity. A detailed discussion on the effect of the discontinuity in the convection-coefficient and source term on the solution of SPBVPs can be found in Farrell *et al.* [133] for ODEs and in O'Riordan and Shishkin [134], and Clavero *et al.* [109] for PDEs. Let $\kappa = \min\{\kappa_1, \kappa_2\}$ and $\gamma = \min\limits_{(x,t)\in D^e} \left\{ \left| \dfrac{b(x,t)}{a(x,t)} \right| \right\}$. Our aim is to develop a parameters uniform numerical scheme for two different cases **I.** $\gamma\varepsilon_1 \leq \kappa\varepsilon_2^2$, and **II.** $\kappa\varepsilon_2^2 \leq \gamma\varepsilon_1$ satisfying assumptions (A1)-(A4). An analogous convergence analysis can be given for the reverse situation of (A1) *i.e.,* for $a(x,t) \geq \kappa_1 > 0$ in D^- and $a(x,t) \leq -\kappa_2 < 0$ in D^+.

The chapter is further organized as follows. In Section 7.2, the minimum principle, and stability estimates are established. Furthermore, the solution decomposition into its regular and singular components is given, and the bounds on the derivatives of the components are also given. The proposed scheme comprising the Crank-Nicolson scheme on a uniform mesh in time and an upwind difference scheme in space on a predefined Shishkin mesh is derived in Section 7.3. A decomposition of the solution of

the fully discrete scheme is given in Section 7.4. Furthermore, the parameters uniform error estimates are also established for both cases. The theoretical results obtained in Section 7.4, are validated through two test problems in Section 7.5. Finally, some concluding remarks on the major finding of the chapter are drawn in the last Section 7.6.

7.2 Continuous Problem

Lemma 7.2.1. *Let $\Phi \in C^2(D^e) \cap C^0(\overline{D})$ be non-negative on Υ and $[\Phi_x](e,t) \leq 0, t > 0$. Then $L\Phi \leq 0$ in D^e gives $\Phi \geq 0$ throughout $\overline{D}$.*

Proof. Define $\Psi(x,t) = e^{\xi|x-e|/2\varepsilon_1}\Phi(x,t)$, $(x,t) \in D$, where $\xi = \kappa_1$ for $x < e$, and $\xi = \kappa_2$ for $x > e$. Assume $\Phi(\theta,\zeta) = \min_{(x,t)\in D^e} \Phi(x,t)$. Then, it is easy to verify that $L\Phi(\theta,\zeta) > 0$ for $\theta \in \Omega^e$, which is a contradiction. Also, if $\theta = e$, then $[\Phi_x](e,\zeta) = [\Psi_x](e,\zeta) - [(\kappa_1+\kappa_2)/(2\varepsilon_1)]\Psi(e,\zeta) > 0$. Thus, we obtain a contradiction. □

Lemma 7.2.2. *The parameter-uniform estimate on $\psi(x,t)$ is given by*

$$\|\psi\|_{\overline{D}} \leq \|\psi\|_{\Upsilon} + \frac{\|f\|_{D^e}}{\beta^*}.$$

Proof. An application of Lemma 7.2.1 to the comparison function

$$\Pi^{\pm}(x,t) = \|\psi\|_{\Upsilon} + \frac{\|f\|_{D^e}}{\beta^*} \pm \psi, \ (x,t) \in \overline{D},$$

yields the required estimate. □

Decomposing the solution ψ as

$$\psi = u + v + w,$$

where the regular component u, and the left and right singular components v and w respectively, satisfy the following BVPs

$$Lu = f, \quad (x,t) \in D^e,$$

with $u(0,t), u(1,t), u(e^-,t), u(e^+,t)$ chosen suitably, and $u(x,0) = \psi_b(x)$, where

$$u(e^-,t) = \lim_{x\to e^-} u(x,t), u(e^+,t) = \lim_{x\to e^+} u(x,t).$$

$$Lv = 0, \quad (x,t) \in D^e,$$

with $v(0,t) = \psi_l(t) - u(0,t) - w(0,t)$, $v(1,t)$ chosen suitably, and $v(x,0) = 0$.

$$Lw = 0, \quad (x,t) \in D^e,$$

with $w(0,t)$ chosen suitably, $w(1,t) = \psi_r(t) - u(1,t) - v(1,t)$, $w(x,0) = 0$.

Lemma 7.2.3. *The layer components for Case I satisfy*

$$|v(x,t)| \le C \begin{cases} \exp((-\kappa\varepsilon_2/\varepsilon_1)x), & \text{if} \quad (x,t) \in D^-, \\ \exp((-\gamma/2\varepsilon_2)(x-e)), & \text{if} \quad (x,t) \in D^+, \end{cases}$$

$$|w(x,t)| \le C \begin{cases} \exp((-\gamma/2\varepsilon_2)(e-x)), & \text{if} \quad (x,t) \in D^-, \\ \exp((-\kappa\varepsilon_2/\varepsilon_1)(1-x)), & \text{if} \quad (x,t) \in D^+. \end{cases}$$

Proof. For the proof, follow the technique given in [105, 134]. □

Lemma 7.2.4. *The layer components for Case II satisfy*

$$|v(x,t)| \le C \begin{cases} \exp\left(-\sqrt{\frac{\kappa\gamma}{\varepsilon_1}}x\right), & \text{if} \quad (x,t) \in D^-, \\ \exp\left(-\frac{1}{2}\sqrt{\frac{\kappa\gamma}{\varepsilon_1}}(x-e)\right), & \text{if} \quad (x,t) \in D^+, \end{cases}$$

$$|w(x,t)| \le C \begin{cases} \exp\left(-\frac{1}{2}\sqrt{\frac{\kappa\gamma}{\varepsilon_1}}(e-x)\right), & \text{if} \quad (x,t) \in D^-, \\ \exp\left(-\sqrt{\frac{\kappa\gamma}{\varepsilon_1}}(1-x)\right), & \text{if} \quad (x,t) \in D^+. \end{cases}$$

Proof. For the proof, follow the technique given in [105, 134]. □

The regular and singular components can be further decomposed as

$$\psi(x,t) = \begin{cases} (u^- + v^- + w_l)(x,t), & \text{if } (x,t) \in D^-, \\ (u^- + v^- + w_l)(e^-,t) = (u^+ + v^+ + w_r)(e^+,t), & \text{if } (x,t) = (e,t), \\ (u^+ + v^+ + w_r)(x,t), & \text{if } (x,t) \in D^+, \end{cases}$$

where u^-, u^+ are the left and right regular components, respectively *i.e.,* u^- and u^+ are the restrictions of u on D^- and D^+ respectively. Similarly, v^-, w_l, the left layer components, and v^+, w_r, are the right layer components, respectively. Thus

$$u(x,t) = \begin{cases} u^-(x,t), & (x,t) \in D^-, \\ u^+(x,t), & (x,t) \in D^+, \end{cases} \qquad v(x,t) = \begin{cases} v^-(x,t), & (x,t) \in D^-, \\ v^+(x,t), & (x,t) \in D^+, \end{cases}$$

$$w(x,t) = \begin{cases} w_l(x,t), & (x,t) \in D^-, \\ w_r(x,t), & (x,t) \in D^+. \end{cases}$$

The proofs of the following theorem on the bounds of the components and their derivatives can be proved in a similar way as given in [135].

Theorem 7.2.1. *The components in Case I, satisfy the following bounds*

$$\left\| \frac{d^k u^-}{dx^k} \right\|_{D^-} \leq C\left(1 + (\varepsilon_1/\varepsilon_2)^{3-k}\right), \left\| \frac{d^k u^+}{dx^k} \right\|_{D^+} \leq C\left(1 + (\varepsilon_1/\varepsilon_2)^{3-k}\right),$$
$$k = 0,1,2,3,4,$$
$$\left\| \frac{d^k v^-}{dx^k} \right\|_{D^-} \leq C(\varepsilon_2/\varepsilon_1)^k, \quad \left\| \frac{d^k v^+}{dx^k} \right\|_{D^+} \leq C\varepsilon_2^{-k}, k = 1,2,3,$$
$$\left\| \frac{d^k w_l}{dx^k} \right\|_{D^-} \leq C\varepsilon_2^{-k}, \left\| \frac{d^k w_r}{dx^k} \right\|_{D^+} \leq C(\varepsilon_2/\varepsilon_1)^k, \; k = 1,2,3.$$

while, in Case II, the bounds are as follows

$$\left\| \frac{d^k u^-}{dx^k} \right\|_{D^-} \leq C\left(1 + \varepsilon_1^{-(k-3)/2}\right), \quad \left\| \frac{d^k u^+}{dx^k} \right\|_{D^+} \leq C\left(1 + \varepsilon_1^{-(k-3)/2}\right),$$
$$k = 0,1,2,3,4,$$
$$\left\| \frac{d^k v^-}{dx^k} \right\|_{D^-} \leq C\varepsilon_1^{-k/2}, \quad \left\| \frac{d^k v^+}{dx^k} \right\|_{D^+} \leq C\varepsilon_1^{-k/2}, \quad k = 1,2,3,4,$$
$$\left\| \frac{d^k w_l}{dx^k} \right\|_{D^-} \leq C\varepsilon_1^{-k/2}, \quad \left\| \frac{d^k w_r}{dx^k} \right\|_{D^+} \leq C\varepsilon_1^{-k/2}, \quad k = 1,2,3,4.$$

7.3 The Discretization

In this section, based on the Crank-Nicolson method an implicit numerical scheme is introduced to solve (7.1). For a fixed time T, the uniform mesh

$$\Lambda^M = \left\{ t_n = n\Delta t : \ n = 0, 1, \ldots, M, \Delta t = \tfrac{T}{M} \right\}$$

is obtained by dividing the time interval $[0, T]$ into M partitions. Then, on $\Omega^e \times \Lambda^M$ the problem (7.1) is semi-discretized as

$$\begin{aligned} -D_t^- Y^{n+1}(x) + \varepsilon_1 (Y^{n+1/2})_{xx}(x) + \varepsilon_2 a^{n+1}(x)(Y^{n+1/2})_x(x) - b^{n+1}(x) Y^{n+1/2}(x) \\ = f^{n+1}(x), x \in \Omega^e, \ 0 \le n \le M-1, \\ Y^{n+1}(0) = \psi_l(t_{n+1}), \ Y^{n+1}(1) = \psi_r(t_{n+1}), \quad 0 \le n \le M-1, \\ Y^0(x) = \psi_b(x), \quad x \in \Omega, \end{aligned}$$

where $Y^{n+1}(x)$ is the approximation of $\psi(x, t_{n+1})$ at $(n+1)$-th time level, D_t^- is the backward difference operator, $Y^{n+1/2}(x) = (Y^{n+1}(x) + Y^n(x))/2$, and $a^{n+1}(x) = a(x, t_{n+1})$, etc.

Rewrite the above equation as

$$\begin{cases} \hat{L} Y^{n+1}(x) = g(x, t_{n+1}), \quad x \in \Omega^e, 0 \le n \le M-1, \\ Y^{n+1}(0) = \psi_l(t_{n+1}), \ Y^{n+1}(1) = \psi_r(t_{n+1}), \quad 0 \le n \le M-1, \\ Y^0(x) = \psi_b(x), \quad x \in \Omega, \end{cases} \tag{7.2}$$

where the operator $\hat{L}$ is defined as

$$\hat{L} \equiv \frac{\varepsilon_1}{2} \frac{d^2}{dx^2} + \varepsilon_2 \frac{a^{n+1}(x)}{2} \frac{d}{dx} - \frac{c^{n+1}(x)}{2} I,$$

and

$$\begin{aligned} g(x, t_{n+1}) &= f^{n+1}(x) - \frac{\varepsilon_1}{2} (Y^n)_{xx}(x) - \varepsilon_2 \frac{a^{n+1}(x)}{2} (Y^n)_x(x) + \frac{d^{n+1}(x)}{2} Y^n(x), \\ c^{n+1}(x) &= b^{n+1}(x) + \frac{2}{\Delta t}, \\ d^{n+1}(x) &= b^{n+1}(x) - \frac{2}{\Delta t}. \end{aligned}$$

The local truncation error in the temporal semi-discretization is given by $e_{j+1} = Y^{n+1}(x) - U(x)$, where $U(x)$ is the computed solution of

$$\begin{cases} \hat{L}U(x) = f(x,t_{n+1}) - \frac{\varepsilon_1}{2}(Y^n)_{xx}(x) - \varepsilon_2 \frac{a(x,t_{n+1})}{2}(Y^n)_x(x) + \frac{d(x,t_{n+1})}{2}Y^n(x), \\ x \in \Omega^e, 0 \le n \le M-1, \\ U(0) = \psi_l(t_{n+1}),\ U(1) = \psi_r(t_{n+1}), \quad 0 \le n \le M-1, \\ U(x) = \psi_b(x), \quad x \in \Omega. \end{cases}$$

The following lemma which estimates the local truncation error T_n can be proved by following the approach given in [136] (see Lemma 3) for one parameter SP-BVPs.

Lemma 7.3.1. *The local truncation error T_n satisfies*

$$\|T_n\| \le C(\Delta t)^3, \quad 0 \le n \le M.$$

The following lemma estimates the global error E_n defined as $E_n = \psi(x,t_n) - Y^{n+1}(x)$ at the instant t_n.

Lemma 7.3.2. *The global error E_n is estimated as*

$$\|E_n\| \le C(\Delta t)^2, \quad 0 \le n \le M.$$

Proof. By definition, we have

$$\begin{aligned} \|E_{n+1}\|_\infty &= \left\| \sum_{k=1}^{n} e_k \right\|_\infty, \quad n \le \frac{T}{\Delta t} \\ &\le \|e_1\|_\infty + \|e_2\|_\infty + \cdots + \|e_n\|_\infty. \end{aligned}$$

Using the previous lemma

$$\|E_{n+1}\|_\infty \le Cn(\Delta t)^3 \le C(\Delta t)^2.$$ □

The solutions

$$\lambda_0(x) = -\frac{\varepsilon_2 a^{n+1}(x)}{2\varepsilon_1} - \sqrt{\left(\frac{\varepsilon_2 a^{n+1}(x)}{2\varepsilon_1}\right)^2 + \frac{c^{n+1}(x)}{\varepsilon_1}} < 0,$$

and

$$\lambda_1(x) = -\frac{\varepsilon_2 a^{n+1}(x)}{2\varepsilon_1} + \sqrt{\left(\frac{\varepsilon_2 a^{n+1}(x)}{2\varepsilon_1}\right)^2 + \frac{c^{n+1}(x)}{\varepsilon_1}} > 0,$$

of the characteristic equation

$$\varepsilon_1 \lambda^2(x) + \varepsilon_2 a^{n+1}(x)\lambda(x) - c^{n+1}(x) = 0,$$

describe the layer behavior of the solution. More precisely, the rate at which the solution decay/rise in the layer region is given by $\eta_0 = -\max_{x\in\overline{\Omega}} \lambda_0(x)$, and $\eta_1 = \min_{x\in\overline{\Omega}} \lambda_1(x)$. In Case I, η_0 and η_1 are of $O\left(\varepsilon_2\varepsilon_1^{-1}\right)$ and $O\left(\varepsilon_2^{-1}\right)$ respectively, while in Case II, both η_0 and η_1 are of $O\left(\varepsilon_1^{-1/2}\right)$.

It is well-known that one can not achieve the uniform convergence on an equidistant mesh for the problems of the form (7.1). Therefore, a non-uniform mesh which is dense in the layer regions will be constructed. To construct the mesh we divide $[0,1]$ into six sub-intervals $[0,\sigma_1]$, $(\sigma_1, e-\sigma_2]$, $(e-\sigma_2, e]$, $(e, e+\sigma_3]$, $(e+\sigma_3, 1-\sigma_4]$, and $(1-\sigma_4, 1]$, where the transition parameters σ_1, σ_2, σ_3, and σ_4 are defined as

$$\sigma_1 = \min\left\{\frac{e}{4}, \frac{\ln N}{\eta_0}\right\}, \quad \sigma_2 = \min\left\{\frac{e}{4}, \frac{\ln N}{\eta_1}\right\},$$

$$\sigma_3 = \min\left\{\frac{1-e}{4}, \frac{\ln N}{\eta_1}\right\}, \quad \sigma_4 = \min\left\{\frac{1-e}{4}, \frac{\ln N}{\eta_0}\right\},$$

where $N \geq 8$ is the number of intervals used for the discretization. In this work in Case I, we have taken, $\eta_0 = \kappa\varepsilon_2/\varepsilon_1$, $\eta_1 = \gamma/2\varepsilon_2$, while in Case II, we have taken $\eta_0 = \sqrt{\kappa\gamma/\varepsilon_1}$, and $\eta_1 = \frac{1}{2}\sqrt{\kappa\gamma/\varepsilon_1}$.

We place $N/8$ points in each of the subintervals $[0,\sigma_1]$, $(e-\sigma_2, e]$, $(e, e+\sigma_3]$, $(e+\sigma_3, 1-\sigma_4]$, and $N/4$ points in $(\sigma_1, e-\sigma_2]$, and $(1-\sigma_4, 1]$. Then, the mesh width is given by

$$h_i = x_i - x_{i-1} = \begin{cases} \dfrac{8\sigma_1}{N}, & \text{if} \quad i = 1,2,\dots\dfrac{N}{8}, \\ \dfrac{4(e-\sigma_1-\sigma_2)}{N}, & \text{if} \quad i = \dfrac{N}{8}+1,\dfrac{N}{8}+2,\dots\dfrac{3N}{8}, \\ \dfrac{8\sigma_2}{N}, & \text{if} \quad i = \dfrac{3N}{8}+1,\dfrac{3N}{8}+2,\dots\dfrac{N}{2}, \\ \dfrac{8\sigma_3}{N}, & \text{if} \quad i = \dfrac{N}{2}+1,\dfrac{N}{2}+2,\dots\dfrac{5N}{8}, \\ \dfrac{4(1-e-\sigma_3-\sigma_4)}{N}, & \text{if} \quad i = \dfrac{5N}{8}+1,\dfrac{5N}{8}+2\dots\dfrac{3N}{4}, \\ \dfrac{8\sigma_4}{N}, & \text{if} \quad i = \dfrac{3N}{4}+1,\dfrac{3N}{4}+2,\dots N, \end{cases}$$

and the mesh points are given by

$$x_i = \begin{cases} \dfrac{8\sigma_1}{N}i, & \text{if} \quad i = 0,1,\dots,\dfrac{N}{8}, \\ \sigma_1 + \dfrac{4(e-\sigma_1-\sigma_2)}{N}\left(i-\dfrac{N}{8}\right), & \text{if} \quad i = \dfrac{N}{8}+1,\dfrac{N}{8}+2,\dots\dfrac{3N}{8}, \\ e-\sigma_2+\dfrac{8\sigma_2}{N}\left(i-\dfrac{3N}{8}\right), & \text{if} \quad i = \dfrac{3N}{8}+1,\dfrac{3N}{8}+2,\dots\dfrac{N}{2}, \\ e+\dfrac{8\sigma_3}{N}\left(i-\dfrac{N}{2}\right), & \text{if} \quad i = \dfrac{N}{2}+1,\dfrac{N}{2}+2,\dots\dfrac{5N}{8}, \\ e+\sigma_3+\dfrac{4(1-e-\sigma_3-\sigma_4)}{N}\left(i-\dfrac{5N}{8}\right), & \text{if} \quad i = \dfrac{5N}{8}+1,\dfrac{5N}{8}+2,\dots\dfrac{3N}{4}, \\ 1-\sigma_4+\dfrac{8\sigma_4}{N}\left(i-\dfrac{3N}{4}\right), & \text{if} \quad i = \dfrac{3N}{4}+1,\dfrac{3N}{4}+2,\dots N. \end{cases}$$

It can be noticed that $x_{N/2} = e$. If we denote $\Omega^{N-} = \{x_i\}_{i=0}^{N/2-1}$, $\Omega^{N+} = \{x_i\}_{i=N/2+1}^{N}$, and $\Omega^N = \{x_i\}_0^N$. Then, the required mesh $D^{N,M}$ is the tensor product of Ω^N and Λ^M *i.e.,* $D^{N,M} = \Omega^N \times \Lambda^M = D^{N-,M} \cup (e \times \Lambda^M) \cup D^{N+,M}$, where $D^{N-,M}$ and $D^{N+,M}$ are the tensor products $\Omega^{N-} \times \Lambda^M$, and $\Omega^{N+} \times \Lambda^M$ respectively. Introducing the operators

$$D_x^- \mu_i^n = \frac{\mu_i^n - \mu_{i-1}^n}{h_i},\ D_x^+ \mu_i^n = \frac{\mu_{i+1}^n - \mu_i^n}{h_{i+1}},\ \text{and}\ \delta_x^2 \mu_i^n = \frac{(D_x^+ - D_x^-)\mu_i^n}{{}_i},$$

where $_i = \frac{h_i+h_{i+1}}{2}$, the full discretization of (7.2) on $D^{N-,M} \cup D^{N+,M}$ is given by

$$\begin{cases} \mathscr{L}^N \widetilde{\psi}(x_i) = \widetilde{g}(x_i), \quad x_i \in \Omega^{N-} \cup \Omega^{N+}, \\ \widetilde{\psi}(x_0) = \psi_l(t_{n+1}), \quad \widetilde{\psi}(x_N) = \psi_r(t_{n+1}), \quad 0 \le n \le M-1, \end{cases} \tag{7.3}$$

where $\widetilde{\psi}(x_i)$ is the approximation of $Y^{n+1}(x_i)$ and the operator $\mathscr{L}^N$ is defined as

$$\mathscr{L}^N \widetilde{\psi} \equiv \frac{\varepsilon_1}{2}\delta_x^2 \widetilde{\psi} + \varepsilon_2 \frac{a^{n+1}}{2} D_x^* \widetilde{\psi} - \frac{c^{n+1}}{2}\widetilde{\psi},$$

$$D_x^* = \begin{cases} D_x^-, & \text{if } i < N/2, \\ D_x^+, & \text{if } i > N/2, \end{cases}$$

and $D_x^- \widetilde{\psi}(x_{N/2}) = D_x^+ \widetilde{\psi}(x_{N/2})$. Moreover, the function $\widetilde{g}(x_i)$ is given by

$$\widetilde{g}(x_i) = f^{n+1}(x_i) - \frac{\varepsilon_1}{2}\delta_x^2 Y^n(x_i) - \varepsilon_2 \frac{a^{n+1}(x_i)}{2} D_x^* Y^n(x_i) + \frac{d^{n+1}(x_i)}{2} Y^n(x_i).$$

7.4 Parameter Uniform Convergence Analysis

Before proving the main result on the convergence of the proposed method, we give some basic properties satisfy by the operator $\mathscr{L}^N$.

Lemma 7.4.1. *Let $\widetilde{\Phi}(x_0) \ge 0$, $\widetilde{\Phi}(x_N) \ge 0$, and $D_x^+\widetilde{\Phi}(x_{N/2}) - D_x^-\widetilde{\Phi}(x_{N/2}) \le 0$. Then, $\mathscr{L}^N\widetilde{\Phi}(x_i) \le 0$ for all $x_i \in \Omega^{N-} \cup \Omega^{N+}$ implies $\widetilde{\Phi}(x_i) \ge 0$ for all $x_i \in \Omega^N$.*

Proof. For contrary assume $\widetilde{\Phi}(l_i) = \min_{x_i \in \Omega^N} \widetilde{\Phi}(x_i) < 0$ for some $l_i \in \Omega^N$. Then, we consider two different cases **(i)** $l_i \in \Omega^{N-} \cup \Omega^{N+}$, and **(ii)** $l_i = e$. In the first case, for $l_i \in \Omega^{N-}$ we have

$$\begin{aligned} \mathscr{L}^N\widetilde{\Phi}(l_i) &= \frac{\varepsilon_1}{2}\delta_x^2\widetilde{\Phi}(l_i) + \varepsilon_2\frac{a^{n+1}(l_i)}{2}D^-\widetilde{\Phi}(l_i) - \frac{c^{n+1}(l_i)}{2}\widetilde{\Phi}(l_i) \\ &= \frac{\varepsilon_1}{2_i}\left(\frac{\widetilde{\Phi}(l_{i+1}) - \widetilde{\Phi}(l_i)}{h_{i+1}} - \frac{\widetilde{\Phi}(l_i) - \widetilde{\Phi}(l_{i-1})}{h_i}\right) \\ &\quad + \varepsilon_2\frac{a^{n+1}(l_i)}{2}\left(\frac{\widetilde{\Phi}(l_i) - \widetilde{\Phi}(l_{i-1})}{h_i}\right) - \frac{c^{n+1}(l_i)}{2}\widetilde{\Phi}(l_i) > 0. \end{aligned}$$

Also, for $l_i \in \Omega^{N+}$ we have

$$\begin{aligned}\mathscr{L}^N\widetilde{\Phi}(l_i) &= \frac{\varepsilon_1}{2}\delta_x^2\widetilde{\Phi}(l_i) + \varepsilon_2\frac{a^{n+1}(l_i)}{2}D^+\widetilde{\Phi}(l_i) - \frac{c^{n+1}(l_i)}{2}\widetilde{\Phi}(l_i)\\ &= \frac{\varepsilon_1}{2_i}\left(\frac{\widetilde{\Phi}(l_{i+1})-\widetilde{\Phi}(l_i)}{h_{i+1}} - \frac{\widetilde{\Phi}(l_i)-\widetilde{\Phi}(l_{i-1})}{h_i}\right)\\ &+ \varepsilon_2\frac{a^{n+1}(l_i)}{2}\left(\frac{\widetilde{\Phi}(l_{i+1})-\widetilde{\Phi}(l_i)}{h_{i+1}}\right) - \frac{c^{n+1}(l_i)}{2}\widetilde{\Phi}(l_i) > 0.\end{aligned}$$

Now in the second case when $l_i = e$, we have $D_x^+\widetilde{\Phi}(x_{N/2}) > 0$ and $D_x^-\widetilde{\Phi}(x_{N/2}) < 0$, so

$$D_x^+\widetilde{\Phi}(x_{N/2}) - D_x^-\widetilde{\Phi}(x_{N/2}) > 0.$$

Thus in both cases, we get a contradiction and the proof is completed. □

We shall now prove the convergence of the proposed scheme for both cases separately. Analogous to the continuous case, decompose the solution $\widetilde{\psi}_i$ of (7.3) into the regular and singular components as

$$\widetilde{\psi}_i = \widetilde{U}_i + \widetilde{V}_i + \widetilde{W}_i.$$

We further decompose the regular component $\widetilde{U}_i$ as $\widetilde{U}_i = \widetilde{U}_i^- + \widetilde{U}_i^+$, where $\widetilde{U}_i^-$ and $\widetilde{U}_i^+$ are the restrictions of $\widetilde{U}_i$ at the left and right side of the point e respectively. Then

$$\mathscr{L}^N\widetilde{U}_i^- = \widetilde{g}(x_i) \text{ in } D^{N-,M}, \quad \widetilde{U}_0^- = u^-(0,t_{n+1}),\ \widetilde{U}_{N/2}^- = u^-(e-,t_{n+1}),$$

and

$$\mathscr{L}^N\widetilde{U}_i^+ = \widetilde{g}(x_i) \text{ in } D^{N+,M}, \quad \widetilde{U}_{N/2}^+ = u^+(e+,t_{n+1}),\ \widetilde{U}_N^+ = u^+(1,t_{n+1}).$$

The layer components $\widetilde{V}_i$ and $\widetilde{W}_i$ are also decomposed as $\widetilde{V}_i = \widetilde{V}_i^- + \widetilde{V}_i^+$, and $\widetilde{W}_i = \widetilde{W}_i^l + \widetilde{W}_i^r$. These components satisfy the following problems

$$\begin{aligned}
\mathscr{L}^N\widetilde{V}_i^- &= 0 \text{ in } D^{N-,M}, \quad \widetilde{V}_0^- = v^-(0,t_{n+1}), \quad \widetilde{V}_{N/2}^- = v^-(e,t_{n+1}),\\
\mathscr{L}^N\widetilde{V}_i^+ &= 0 \text{ in } D^{N+,M}, \quad \widetilde{V}_{N/2}^+ = v^+(e,t_{n+1}), \quad \widetilde{V}_N^+ = 0,\\
\mathscr{L}^N\widetilde{W}_i^l &= 0 \text{ in } D^{N-,M}, \quad \widetilde{W}_0^l = 0, \quad \widetilde{W}_{N/2}^l = w_l(e,t_{n+1}),\\
\mathscr{L}^N\widetilde{W}_i^r &= 0 \text{ in } D^{N+,M}, \quad \widetilde{W}_{N/2}^r = 0, \quad \widetilde{W}_N^r = w_r(1,t_{n+1}),\\
(\widetilde{U}_i^- + \widetilde{V}_i^- + \widetilde{W}_i^l)(e,t_{n+1}) &= (\widetilde{U}_i^+ + \widetilde{V}_i^+ + \widetilde{W}_i^r)(e,t_{n+1}).
\end{aligned}$$

Lemma 7.4.2. *The bounds for the singular components are given as*

$$\begin{aligned}
|\widetilde{V}_i^-| &\le C\prod_{j=1}^{i}(1+\eta_0 h_j)^{-1}, \quad i = 0,1,\ldots,N/2,\\
|\widetilde{V}_i^+| &\le C\prod_{j=N/2+1}^{i}(1+\eta_1 h_j)^{-1}, \quad i = N/2+1,\ldots,N,\\
|\widetilde{W}_i^l| &\le C\prod_{j=i+1}^{N/2}(1+\eta_1 h_j)^{-1}, \quad i = 0,1,\ldots,N/2,\\
|\widetilde{W}_i^r| &\le C\prod_{j=i+1}^{N}(1+\eta_0 h_j)^{-1}, \quad i = N/2+1,\ldots,N,
\end{aligned}$$

where η_0 and η_1 are defined in the previous section.

Proof. Refer, [135]. □

The nodal error is given by $\nu_{i,n+1} = (u(x_i,t_{n+1}) - \widetilde{U}_i) + (v(x_i,t_{n+1}) - \widetilde{V}_i) + (w(x_i,t_{n+1}) - \widetilde{W}_i)$.

Analysis for Case I ($\gamma\varepsilon_1 \le \kappa\varepsilon_2^2$). The error estimate is obtained by estimating the errors in the smooth and singular components separately.

Lemma 7.4.3. *The error bound for the regular component is given by*

$$|u(x_i,t_{n+1}) - \widetilde{U}_i|_{\Omega^{N-}\cup\Omega^{N+}} \le CN^{-1}.$$

Proof. Using the classical argument on the domain Ω^{N-}, we obtain

$$\begin{aligned}|\mathscr{L}^N(u^-(x_i,t_{n+1})-\widetilde{U}_i^-)| &\leq CN^{-1}(\varepsilon_1\|u^-\|_3+\varepsilon_2\|a\|\|u^-\|_2)\\ &\leq CN^{-1}.\end{aligned}$$

Thus an application of Lemma 7.4.1 gives

$$|u^-(x_i,t_{n+1})-\widetilde{U}_i^-|\leq CN^{-1}.$$

The same error bound can be obtained by using the above argument on the domain Ω^{N+} *i.e.,*

$$|u^+(x_i,t_{n+1})-\widetilde{U}_i^+|\leq CN^{-1}.$$

Hence, the error bound for the regular component is given by

$$|u(x_i,t_{n+1})-\widetilde{U}_i|_{\Omega^{N-}\cup\Omega^{N+}}\leq CN^{-1}.$$ □

Lemma 7.4.4. *The error bound for the left interior layer component in the domain* Ω^{N-} *is given by*

$$|v^-(x_i,t_{n+1})-\widetilde{V}_i^-|\leq CN^{-1}(\ln N)^2.$$

Proof. If $x_i\in[0,\sigma_1)$, then for $\sigma_1=e/4$, we have $\varepsilon_2/\varepsilon_1\leq C\ln N$ and so using the classical argument, we obtain

$$\begin{aligned}|\mathscr{L}^N(v^-(x_i,t_{n+1})-\widetilde{V}_i^-)| &\leq CN^{-1}(\varepsilon_1\|v^-\|_3+\varepsilon_2\|a\|\|v^-\|_2)\\ &\leq CN^{-1}(\ln N)^2.\end{aligned}$$

Now for $\sigma_1<e/4$, the classical argument gives

$$\begin{aligned}|\mathscr{L}^N(v^-(x_i,t_{n+1})-\widetilde{V}_i^-)| &\leq C(h_i+h_{i+1})(\varepsilon_1\|v^-\|_3+\varepsilon_2\|a\|\|v^-\|_2)\\ &\leq CN^{-1}\sigma_1(\varepsilon_1\|v^-\|_3+\varepsilon_2\|a\|\|v^-\|_2)\\ &\leq C\frac{\varepsilon_2^2}{\varepsilon_1}N^{-1}\ln N.\end{aligned}$$

Consider $\Phi(x) = C(N^{-1} + N^{-1}\ln N(\sigma_1 - x)\frac{\varepsilon_2}{\varepsilon_1})$. Then it is easy to obtain

$$\mathscr{L}^N\Phi_i = -\left(\frac{c^{n+1}}{2}\Phi_i + C\frac{\varepsilon_2^2}{\varepsilon_1}N^{-1}\ln N\right) \leq -|\mathscr{L}^N(v^-(x_i,t_{n+1}) - \widetilde{V}_i^-)|,$$

which gives

$$\begin{aligned}|v^-(x_i,t_{n+1}) - \widetilde{V}_i^-| &= C\left(N^{-1} + (N^{-1}\ln N)(\sigma_1 - x_i)\frac{\varepsilon_2}{\varepsilon_1}\right)\\ &\leq C\left(N^{-1} + (N^{-1}\ln N)\sigma_1\frac{\varepsilon_2}{\varepsilon_1}\right)\\ &\leq CN^{-1}(\ln N)^2. \end{aligned} \tag{7.4}$$

Furthermore, for $x_i \in [\sigma_1, e)$, we have

$$|v^-(x_i,t_{n+1}) - \widetilde{V}_i^-| \leq |v^-(x_i,t_{n+1})| + |\widetilde{V}_i^-|.$$

Now Lemma 7.4.2 for $i = N/8$, and the fact $\ln(1+y) > y(1-y/2)$, gives $|\widetilde{V}_i^-| \leq CN^{-1}$, $\forall x_i \in [\sigma_1, e)$. Also,

$$\begin{aligned}|v^-(x_i,t_{n+1})| &\leq C\exp((-\kappa\varepsilon_2/\varepsilon_1)x_i)\\ &\leq C\exp((-\kappa\varepsilon_2/\varepsilon_1)\sigma_1)\\ &\leq C\exp((-\kappa\varepsilon_2/\varepsilon_1)(\ln N/\eta_0))\\ &\leq CN^{-1}.\end{aligned}$$

Hence, for $x_i \in [\sigma_1, e)$

$$|v^-(x_i,t_{n+1}) - \widetilde{V}_i^-| \leq CN^{-1}. \tag{7.5}$$

Finally, on combining (7.4) and (7.5), we get

$$|v^-(x_i,t_{n+1}) - \widetilde{V}_i^-|_{\Omega^{N-}} \leq CN^{-1}(\ln N)^2. \qquad \square$$

Lemma 7.4.5. *The error bound for the right interior layer component is given by*

$$|v^+(x_i,t_{n+1}) - \widetilde{V}_i^+|_{\Omega^{N+}} \leq CN^{-1}(\ln N)^2.$$

Proof. For the uniform mesh, the proof is similar as for the left interior layer component. In the case of non-uniform mesh, when $x_i \in [e+\sigma_3, 1)$, we have

$$|v^+(x_i,t_{n+1}) - \widetilde{V}_i^+| \leq |v^+(x_i,t_{n+1})| + |\widetilde{V}_i^+|.$$

Now Lemma 7.4.2 for $i = 5N/8$, and the fact $\ln(1+y) > y(1-y/2)$, gives $|\widetilde{V}_i^+| \leq CN^{-1}$, $\forall x_i \in [e+\sigma_3, 1)$. Also,

$$\begin{aligned}
|v^+(x_i,t_{n+1})| &\leq C\exp(-(\gamma/2\varepsilon_2)(x_i-e)) \\
&\leq C\exp(-(\gamma/2\varepsilon_2)\sigma_3) \\
&\leq C\exp(-(\gamma/2\varepsilon_2)(\ln N/\eta_1)) \\
&\leq CN^{-1}.
\end{aligned}$$

Hence, for $x_i \in [e+\sigma_3, 1)$

$$|v^+(x_i,t_{n+1}) - \widetilde{V}_i^+| \leq CN^{-1}. \tag{7.6}$$

Now for $x_i \in [e, e+\sigma_3)$, the truncation error bound gives

$$\begin{aligned}
|\mathscr{L}^N(v^+(x_i,t_{n+1}) - \widetilde{V}_i^+)| &\leq C(h_i+h_{i+1})(\varepsilon_1\|v^+\|_3 + \varepsilon_2\|a\|\|v^+\|_2) \\
&\leq CN^{-1}\sigma_3(\varepsilon_1\|v^+\|_3 + \varepsilon_2\|a\|\|v^+\|_2) \\
&\leq CN^{-1}\sigma_3(\varepsilon_1\varepsilon_2^{-3} + \varepsilon_2\varepsilon_2^{-2}) \\
&\leq CN^{-1}(\ln N/\eta_1)(\varepsilon_1\varepsilon_2^{-3} + \varepsilon_2\varepsilon_2^{-2}) \\
&\leq CN^{-1}\ln N.
\end{aligned}$$

Use of the discrete minimum principle, yields

$$|v^+(x_i,t_{n+1}) - \widetilde{V}_i^+| \leq CN^{-1}\ln N. \tag{7.7}$$

Finally, on combining (7.6) and (7.7), we get

$$|v^+(x_i,t_{n+1}) - \widetilde{V}_i^+|_{\Omega^{N+}} \leq CN^{-1}\ln N. \qquad \square$$

The error bound on the interior layer component is given in the following lemma by combining Lemma 7.4.4 and Lemma 7.4.5.

Lemma 7.4.6. *At each mesh point in $\Omega^{N-} \cup \Omega^{N+}$, the error bound satisfies*

$$\max_{x_i \in \Omega^{N-} \cup \Omega^{N+}} |v(x_i, t_{n+1}) - \widetilde{V}_i| \leq CN^{-1}(\ln N)^2.$$

The similar error bound can be obtained for the boundary layer component and is given by

Lemma 7.4.7. *At each mesh point in $\Omega^{N-} \cup \Omega^{N+}$, the error bound satisfies*

$$\max_{x_i \in \Omega^{N-} \cup \Omega^{N+}} |w(x_i, t_{n+1}) - \widetilde{W}_i| \leq CN^{-1}(\ln N)^2.$$

Analysis for Case II ($\kappa\varepsilon_2^2 \leq \gamma\varepsilon_1$).

Lemma 7.4.8. *The error bound for the regular component is given by*

$$|u(x_i, t_{n+1}) - \widetilde{U}_i|_{\Omega^{N-} \cup \Omega^{N+}} \leq CN^{-1}.$$

Proof. For $x_i \in \Omega^{N-}$, we have

$$\begin{aligned} |\mathscr{L}^N(u^-(x_i, t_{n+1}) - \widetilde{U}_i^-)| &\leq CN^{-1}(\varepsilon_1 \|u^-\|_3 + \varepsilon_2 \|a\| \|u^-\|_2) \\ &\leq CN^{-1}. \end{aligned}$$

Using Lemma 7.4.1, we get the following estimate

$$|u^-(x_i, t_{n+1}) - \widetilde{U}_i^-| \leq CN^{-1}.$$

The similar error bound can be obtained for the domain Ω^{N+} and is given by

$$|u^+(x_i, t_{n+1}) - \widetilde{U}_i^+| \leq CN^{-1}.$$

Hence, the error bound for the regular component is given by

$$|u(x_i, t_{n+1}) - \widetilde{U}_i|_{\Omega^{N-} \cup \Omega^{N+}} \leq CN^{-1}.$$ □

Lemma 7.4.9. *The error bound for the left interior layer component is given by*

$$|v^-(x_i, t_{n+1}) - \widetilde{V}_i^-|_{\Omega^{N-}} \leq CN^{-1} \ln N.$$

Proof. For $x_i \in [0, \sigma_1)$, the classical argument gives

$$\begin{aligned}|\mathscr{L}^N(v^-(x_i,t_{n+1}) - \widetilde{V}_i^-)| &\leq C(h_i + h_{i+1})(\varepsilon_1\|v^-\|_3 + \varepsilon_2\|a\|\|v^-\|_2)\\ &\leq CN^{-1}\sigma_1(\varepsilon_1\|v^-\|_3 + \varepsilon_2\|a\|\|v^-\|_2)\\ &\leq CN^{-1}(\ln N/\eta_0)(\varepsilon_1\varepsilon_1^{-3/2} + \varepsilon_2\varepsilon_1^{-1})\\ &\leq CN^{-1}\ln N.\end{aligned}$$

Using Lemma 7.4.1, we get the following estimate

$$|v^-(x_i,t_{n+1}) - \widetilde{V}_i^-| \leq CN^{-1}\ln N. \tag{7.8}$$

Furthermore, for $x_i \in [\sigma_1, e)$, we have

$$|v^-(x_i,t_{n+1}) - \widetilde{V}_i^-| \leq |v^-(x_i,t_{n+1})| + |\widetilde{V}_i^-|.$$

Now Lemma 7.4.2 for $i = N/8$, and the fact $\ln(1+y) > y(1-y/2)$, gives $|\widetilde{V}_i^-| \leq CN^{-1}$, $\forall x_i \in [\sigma_1, e)$. Also,

$$\begin{aligned}|v^-(x_i,t_{n+1})| &\leq C\exp\left(-\sqrt{\frac{\kappa\gamma}{\varepsilon_1}}x_i\right)\\ &\leq C\exp\left(-\sqrt{\frac{\kappa\gamma}{\varepsilon_1}}\sigma_1\right)\\ &\leq CN^{-1}.\end{aligned}$$

Hence, for $x_i \in [\sigma_1, e)$

$$|v^-(x_i,t_{n+1}) - \widetilde{V}_i^-| \leq CN^{-1}. \tag{7.9}$$

Finally, combining (7.8) and (7.9), we get

$$|v^-(x_i,t_{n+1}) - \widetilde{V}_i^-|_{\Omega^{N-}} \leq CN^{-1}\ln N. \qquad \square$$

Lemma 7.4.10. *The error bound for the right interior layer component is given by*

$$|v^+(x_i,t_{n+1}) - \widetilde{V}_i^+|_{\Omega^{N+}} \leq CN^{-1}\ln N.$$

Proof. For the case of non-uniform mesh, for $x_i \in [e+\sigma_3, 1)$, we have

$$|v^+(x_i,t_{n+1}) - \widetilde{V}_i^+| \leq |v^+(x_i,t_{n+1})| + |\widetilde{V}_i^+|.$$

Now Lemma 7.4.2 for $i = 5N/8$, and the fact $\ln(1+y) > y(1-y/2)$, gives $|\widetilde{V}_i^+| \leq CN^{-1}$, $\forall\, x_i \in [e+\sigma_3, 1)$. Also,

$$\begin{aligned}
|v^+(x_i,t_{n+1})| &\leq C\exp\left(-\frac{1}{2}\sqrt{\frac{\kappa\gamma}{\varepsilon_1}}(x_i-e)\right)\\
&\leq C\exp\left(-\frac{1}{2}\sqrt{\frac{\kappa\gamma}{\varepsilon_1}}\sigma_3\right)\\
&\leq CN^{-1}.
\end{aligned}$$

Hence, for $x_i \in [e+\sigma_3, 1)$

$$|v^+(x_i,t_{n+1}) - \widetilde{V}_i^+| \leq CN^{-1}. \tag{7.10}$$

Now for $x_i \in [e, e+\sigma_3)$, the classical argument gives

$$\begin{aligned}
|\mathscr{L}^N(v^+(x_i,t_{n+1}) - \widetilde{V}_i^+)| &\leq C(h_i+h_{i+1})(\varepsilon_1\|v^+\|_3 + \varepsilon_2\|a\|\|v^+\|_2)\\
&\leq CN^{-1}\sigma_3(\varepsilon_1\|v^+\|_3 + \varepsilon_2\|a\|\|v^+\|_2)\\
&\leq CN^{-1}\sigma_3(\varepsilon_1\varepsilon_1^{-3/2} + \varepsilon_2\|a\|\varepsilon_1^{-1})\\
&\leq CN^{-1}(\ln N/\eta_1)(\varepsilon_1^{-1/2} + \varepsilon_2\|a\|\varepsilon_1^{-1})\\
&\leq CN^{-1}\ln N.
\end{aligned}$$

Using Lemma 7.4.1, we get the following estimate

$$|v^+(x_i,t_{n+1}) - \widetilde{V}_i^+| \leq CN^{-1}\ln N. \tag{7.11}$$

Finally, on combining (7.10) and (7.11), we get

$$|v^+(x_i,t_{n+1}) - \widetilde{V}_i^+|_{\Omega^{N+}} \leq CN^{-1}\ln N. \qquad \square$$

Thus, the error bound on the interior layer component is given by combining Lemma 7.4.9 and Lemma 7.4.10.

Lemma 7.4.11. *The error bound for the interior layer component is given by*

$$\max_{x_i \in \Omega^{N-} \cup \Omega^{N+}} |v(x_i, t_{n+1}) - \widetilde{V}_i| \leq CN^{-1} \ln N.$$

The error bound on the boundary layer component given in the following lemma can be obtained in the same way.

Lemma 7.4.12. *The error bound for the boundary layer component is given by*

$$\max_{x_i \in \Omega^{N-} \cup \Omega^{N+}} |w(x_i, t_{n+1}) - \widetilde{W}_i| \leq CN^{-1} \ln N.$$

Theorem 7.4.1. *The solution $\psi(x,t)$ of (7.1) and $\widetilde{\psi}_i$ of (7.3) satisfy the following parameter-uniform error estimate*

$$\sup_{0<\varepsilon_1,\varepsilon_2 \ll 1} \max_{\substack{1 \leq i \leq N \\ 1 \leq n \leq M}} |\psi(x_i, t_n) - \widetilde{\psi}_i| \leq C \begin{cases} ((\Delta t)^2 + N^{-1}(\ln N)^2), & \textit{Case I}, \\ ((\Delta t)^2 + N^{-1} \ln N), & \textit{Case II}. \end{cases}$$

Proof. The proof for $x_i \neq e$ follows from the triangle inequality and Lemmas 7.3.2, 7.4.3, 7.4.6, 7.4.7, 7.4.8, 7.4.11 and 7.4.12. The proof for $x_i = e$ can be done by following the technique given in [137]. □

7.5 Numerical Illustrations

For fixed ε_1, ε_2, the maximum point-wise absolute error is calculated as

$$e^{N,M}_{\varepsilon_1,\varepsilon_2} = \max_n \left(\max_i |\widetilde{\psi}^{2N,2M}_{2i} - \widetilde{\psi}^{N,M}_i| \right),$$

where $\widetilde{\psi}^{N,M}_i$, and $\widetilde{\psi}^{2N,2M}_{2i}$ are the solutions on the mesh $D^{N,M}$ and $\hat{D}^{2N,2M}$, respectively. Since the values of the transition parameters σ_i, $i = 1,2,3,4$ are different in the cases of N and $2N$ mesh intervals, so the fine mesh $\hat{D}^{2N,2M}$ is obtained by inserting one nodal point between two consecutive nodal points (in $D^{N,M}$) in both directions. Moreover, the order of convergence $\rho^{N,M}_{\varepsilon_1,\varepsilon_2}$ is calculated as

$$\rho^{N,M}_{\varepsilon_1,\varepsilon_2} = \log_2 \left(\frac{e^{N,M}_{\varepsilon_1,\varepsilon_2}}{e^{2N,2M}_{\varepsilon_1,\varepsilon_2}} \right).$$

Example 7.5.1. In the following problem, we take $\Omega = (0,1)$, $\Lambda = (0,1]$ and $e = 0.5$

$$-\psi_t + \varepsilon_1 \psi_{xx} + \varepsilon_2 a(x,t)\psi_x - b(x,t)\psi = f(x,t),\ (x,t) \in D^e,$$
$$\psi_l(t) = 0 \text{ on } \Upsilon_l, \quad \psi_r(t) = 0 \text{ on } \Upsilon_r, \quad \psi_b(x) = 0 \text{ on } \Upsilon_b,$$

where $a(x,t)$ is $-(1+x(1-x))$ and $1+x(1-x)$ in D^- and D^+ respectively; $b(x,t) = 1+\exp(x)$ in D^e; and $f(x,t)$ is $-2(1+x^2)t$ and $2(1+x^2)t$ in D^- and D^+, respectively.

Example 7.5.2. Again, we take $\Omega = (0,1)$, $\Lambda = (0,1]$ and $e = 0.5$ for the following problem

$$-\psi_t + \varepsilon_1 \psi_{xx} + \varepsilon_2 a(x,t)\psi_x - b(x,t)\psi = f(x,t),\ (x,t) \in D^e,$$
$$\psi_l(t) = 0 \text{ on } \Upsilon_l, \quad \psi_r(t) = 0 \text{ on } \Upsilon_r, \quad \psi_b(x) = 0 \text{ on } \Upsilon_b,$$

where $a(x,t)$ is $-(1+\exp(-xt))$ and $2+x+t$ in D^- and D^+ respectively; $b(x,t) = 2+xt$ in D^e; and $f(x,t)$ is $(\exp(t^2)-1)(1+xt)$ and $-(2+x)t^2$ in D^- and D^+, respectively.

To verify the theoretical estimates, the numerical results obtained on a specific range $\mathscr{R}(\varepsilon_1, \varepsilon_2)$ of the perturbation parameters satisfying either Case I or Case II are presented in the tables. Note that the cases σ_1, $\sigma_2 = e/4$ and σ_3, $\sigma_4 = (1-e)/4$ occur for a small subset of $\mathscr{R}(\varepsilon_1, \varepsilon_2)$ of perturbation parameters, and the uniform mesh is sufficient to obtain good accuracy. It can be noticed that in Case I, the problem considered in this study is similar to the convection-diffusion problem, however, in Case II it becomes similar to the reaction-diffusion problem.

Table 7.1: $e^{N,M}_{\varepsilon_1,\varepsilon_2}$ and $\rho^{N,M}_{\varepsilon_1,\varepsilon_2}$ for Example 7.5.1 for $\varepsilon_1 = 2^{-6}$.

	N						
ε_2	64	128	256	512	1024	2048	4096
2^{-6}	3.28e-03	1.68e-03	8.53e-04	4.30e-04	2.16e-04	1.08e-04	5.41e-05
	0.96	0.98	0.99	0.99	1.00	1.00	
2^{-10}	3.40e-03	1.75e-03	8.90e-04	4.48e-04	2.25e-04	1.13e-04	5.64e-05
	0.96	0.97	0.99	0.99	0.99	1.00	
2^{-14}	3.41e-03	1.76e-03	8.92e-04	4.49e-04	2.26e-04	1.13e-04	5.66e-05
	0.95	0.98	0.99	0.99	1.00	1.00	
2^{-18}	3.41e-03	1.76e-03	8.92e-04	4.50e-04	2.26e-04	1.13e-04	5.66e-05
	0.95	0.98	0.99	0.99	1.00	1.00	
2^{-22}	3.41e-03	1.76e-03	8.92e-04	4.50e-04	2.26e-04	1.13e-04	5.66e-05
	0.95	0.98	0.99	0.99	1.00	1.00	
2^{-26}	3.41e-03	1.76e-03	8.92e-04	4.50e-04	2.26e-04	1.13e-04	5.66e-05
	0.95	0.98	0.99	0.99	1.00	1.00	
2^{-30}	3.41e-03	1.76e-03	8.92e-04	4.50e-04	2.26e-04	1.13e-04	5.66e-05
	0.95	0.98	0.99	0.99	1.00	1.00	

Table 7.2: $e^{N,M}_{\varepsilon_1,\varepsilon_2}$ and $\rho^{N,M}_{\varepsilon_1,\varepsilon_2}$ for Example 7.5.1 for $\varepsilon_2 = 2^{-8}$.

	N						
ε_1	64	128	256	512	1024	2048	4096
2^{-18}	3.15e-02	1.97e-02	1.19e-02	6.78e-03	3.78e-03	2.09e-03	1.09e-03
	0.68	0.73	0.81	0.84	0.85	0.94	
2^{-20}	4.30e-02	2.87e-02	1.92e-02	1.19e-02	6.87e-03	3.87e-03	2.04e-03
	0.58	0.58	0.69	0.79	0.83	0.92	
2^{-22}	4.72e-02	3.29e-02	2.31e-02	1.46e-02	8.63e-03	4.93e-03	2.48e-03
	0.52	0.51	0.66	0.76	0.81	0.99	
2^{-24}	4.84e-02	3.42e-02	2.43e-02	1.55e-02	9.22e-03	5.29e-03	2.65e-03
	0.50	0.49	0.65	0.75	0.80	1.00	
2^{-26}	4.87e-02	3.46e-02	2.47e-02	1.57e-02	9.38e-03	5.39e-03	2.69e-03
	0.49	0.49	0.65	0.74	0.80	1.00	
2^{-28}	4.88e-02	3.47e-02	2.47e-02	1.58e-02	9.42e-03	5.41e-03	2.71e-03
	0.49	0.49	0.65	0.75	0.76	1.00	
2^{-32}	4.88e-02	3.47e-02	2.47e-02	1.58e-02	9.42e-03	5.41e-03	2.71e-03
	0.49	0.49	0.65	0.75	0.80	1.00	

Table 7.3: $e^{N,M}_{\varepsilon_1,\varepsilon_2}$ and $\rho^{N,M}_{\varepsilon_1,\varepsilon_2}$ for Example 7.5.1 by taking $N = 256$.

$\varepsilon_2 \downarrow / \varepsilon_1 \rightarrow$	2^{-6}	2^{-10}	2^{-14}	2^{-18}	2^{-22}	2^{-26}	2^{-30}
2^{-6}	8.53e-04	2.51e-03	1.20e-02	2.33e-02	2.49e-02	2.50e-02	2.50e-02
2^{-10}	8.90e-04	9.80e-04	1.55e-03	3.89e-03	1.18e-02	2.31e-02	2.46e-02
2^{-14}	8.92e-04	9.80e-04	1.00e-03	1.01e-03	1.54e-03	3.89e-03	1.18e-02
2^{-18}	8.92e-04	9.80e-04	1.00e-03	1.01e-03	1.02e-03	1.02e-03	1.54e-03
2^{-22}	8.92e-04	9.80e-04	1.00e-03	1.01e-03	1.02e-03	1.02e-03	1.02e-03
2^{-26}	8.92e-04	9.80e-04	1.00e-03	1.01e-03	1.02e-03	1.02e-03	1.02e-03
2^{-30}	8.92e-04	9.80e-04	1.00e-03	1.01e-03	1.02e-03	1.02e-03	1.02e-03

Table 7.4: Comparison of $e^{N,M}_{\varepsilon_1,\varepsilon_2}$ for Example 7.5.1 for $\varepsilon_2 = 2^{-4}$

	$N = 64$		$N = 128$		$N = 256$		$N = 512$	
ε_1	In [114]	PM	In [114]	PM	In [114]	PM	In [114]	PM
2^{-6}	4.28e-03	3.04e-03	1.87e-03	1.55e-03	8.63e-04	7.83e-04	4.14e-04	3.94e-04
2^{-10}	3.64e-02	1.86e-02	1.84e-02	1.23e-02	8.96e-03	7.52e-03	5.14e-03	4.46e-03
2^{-14}	7.63e-02	2.98e-02	4.69e-02	1.80e-02	2.62e-02	1.08e-02	1.39e-02	6.35e-03
2^{-18}	8.23e-02	3.13e-02	5.23e-02	1.93e-02	3.00e-02	1.18e-02	1.63e-02	6.94e-03
2^{-22}	8.27e-02	3.14e-02	5.27e-02	1.94e-02	3.03e-02	1.19e-02	1.65e-02	6.98e-03

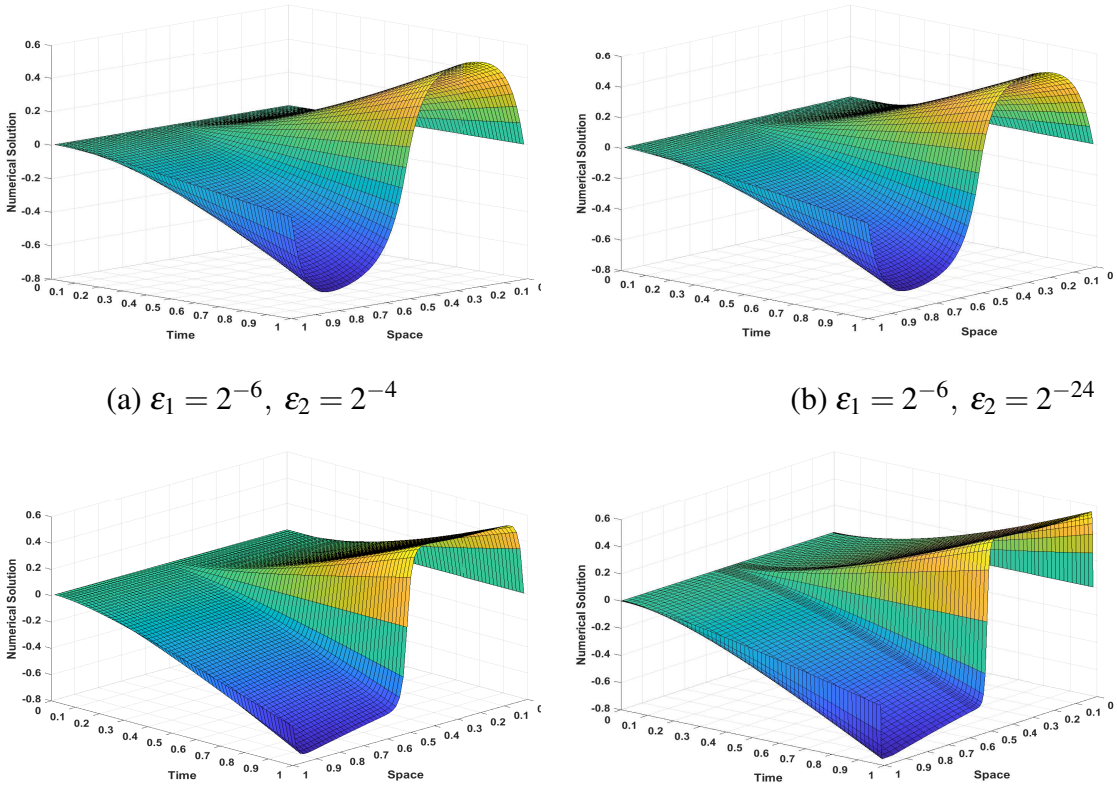

(a) $\varepsilon_1 = 2^{-6},\ \varepsilon_2 = 2^{-4}$ (b) $\varepsilon_1 = 2^{-6},\ \varepsilon_2 = 2^{-24}$

(c) $\varepsilon_1 = 2^{-10},\ \varepsilon_2 = 2^{-8}$ (d) $\varepsilon_1 = 2^{-15},\ \varepsilon_2 = 2^{-6}$

Figure 7.1: Numerical solution profiles for Example 7.5.1.

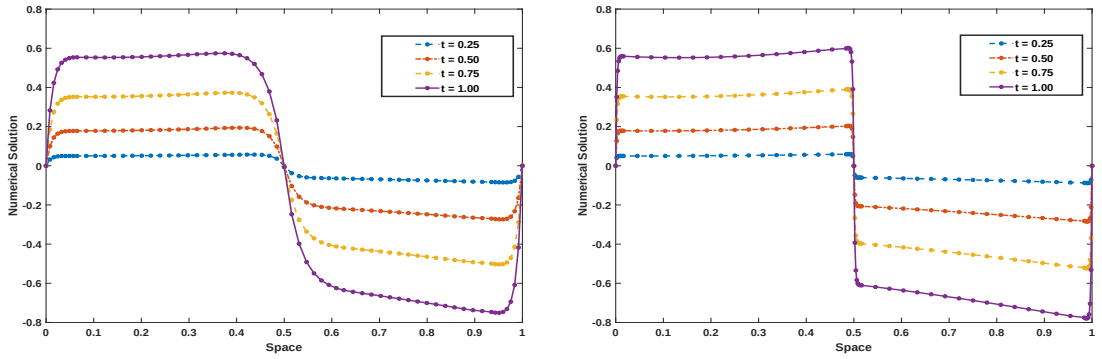

(a) $\varepsilon_1 = 2^{-10},\ \varepsilon_2 = 2^{-4}$ (b) $\varepsilon_1 = 2^{-16},\ \varepsilon_2 = 2^{-24}$

Figure 7.2: Numerical solution profiles for Example 7.5.1.

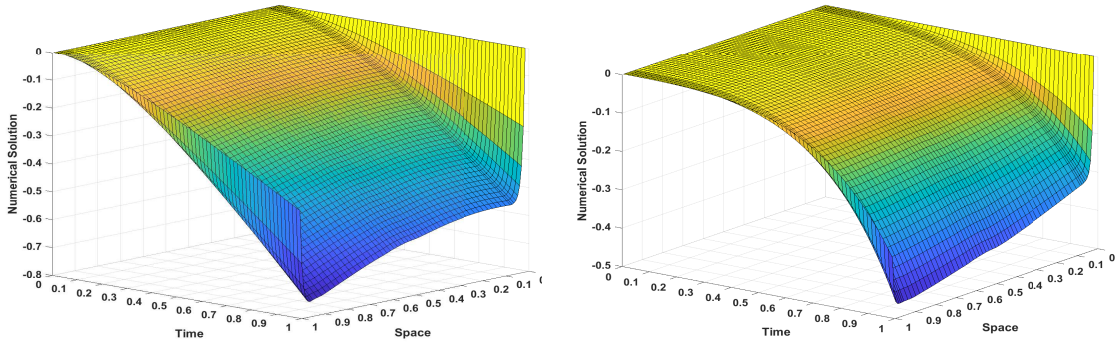

(a) Example 7.5.1 (b) Example 7.5.2

Figure 7.3: Numerical solution profiles for $\varepsilon_1 = 2^{-10}$, $\varepsilon_2 = 2^{-4}$ by taking continuous source terms.

Table 7.5: $e^{N,M}_{\varepsilon_1,\varepsilon_2}$ and $\rho^{N,M}_{\varepsilon_1,\varepsilon_2}$ for Example 7.5.2 for $\varepsilon_1 = 2^{-15}$.

	N						
ε_2	32	64	128	256	512	1024	2048
2^{-6}	3.48e-02	3.83e-02	3.16e-02	2.20e-02	1.45e-02	8.90e-03	5.19e-03
	-0.14	0.28	0.52	0.60	0.70	0.78	
2^{-10}	1.43e-02	7.55e-03	4.17e-03	2.35e-03	1.30e-03	7.16e-04	3.95e-04
	0.92	0.86	0.83	0.85	0.86	0.86	
2^{-14}	1.21e-02	5.83e-03	3.02e-03	1.54e-03	7.77e-04	3.90e-04	1.96e-04
	1.05	0.95	0.97	0.99	0.99	0.99	
2^{-18}	1.20e-02	5.84e-03	3.02e-03	1.54e-03	7.77e-04	3.90e-04	1.96e-04
	1.04	0.95	0.97	0.99	0.99	0.99	
2^{-22}	1.20e-02	5.84e-03	3.02e-03	1.54e-03	7.77e-04	3.90e-04	1.96e-04
	1.04	0.95	0.97	0.99	0.99	0.99	
2^{-26}	1.20e-02	5.84e-03	3.02e-03	1.54e-03	7.77e-04	3.90e-04	1.96e-04
	1.04	0.95	0.97	0.99	0.99	0.99	
2^{-30}	1.20e-02	5.84e-03	3.02e-03	1.54e-03	7.77e-04	3.90e-04	1.96e-04
	1.04	0.95	0.97	0.99	0.99	0.99	

Table 7.6: $e^{N,M}_{\varepsilon_1,\varepsilon_2}$ and $\rho^{N,M}_{\varepsilon_1,\varepsilon_2}$ for Example 7.5.2 for $\varepsilon_2 = 2^{-16}$.

	N						
ε_1	32	64	128	256	512	1024	2048
2^{-4}	7.44e-03	3.94e-03	2.03e-03	1.03e-03	5.22e-04	2.62e-04	1.31e-04
	0.92	0.96	0.98	0.98	0.99	1.00	
2^{-8}	1.02e-02	5.40e-03	2.79e-03	1.42e-03	7.17e-04	3.60e-04	1.81e-04
	0.92	0.95	0.97	0.99	0.99	0.99	
2^{-12}	1.15e-02	5.92e-03	2.98e-03	1.51e-03	7.63e-04	3.83e-04	1.92e-04
	0.96	0.99	0.98	0.98	0.99	1.00	
2^{-16}	1.21e-02	5.83e-03	3.03e-03	1.54e-03	7.79e-04	3.92e-04	1.96e-04
	1.05	0.94	0.98	0.98	0.99	1.00	
2^{-20}	1.23e-02	5.91e-03	3.05e-03	1.56e-03	7.85e-04	3.95e-04	1.98e-04
	1.06	0.95	0.97	0.99	0.99	1.00	
2^{-24}	1.30e-02	5.97e-03	3.06e-03	1.56e-03	7.89e-04	3.96e-04	1.99e-04
	1.12	0.96	0.97	0.98	0.99	0.99	

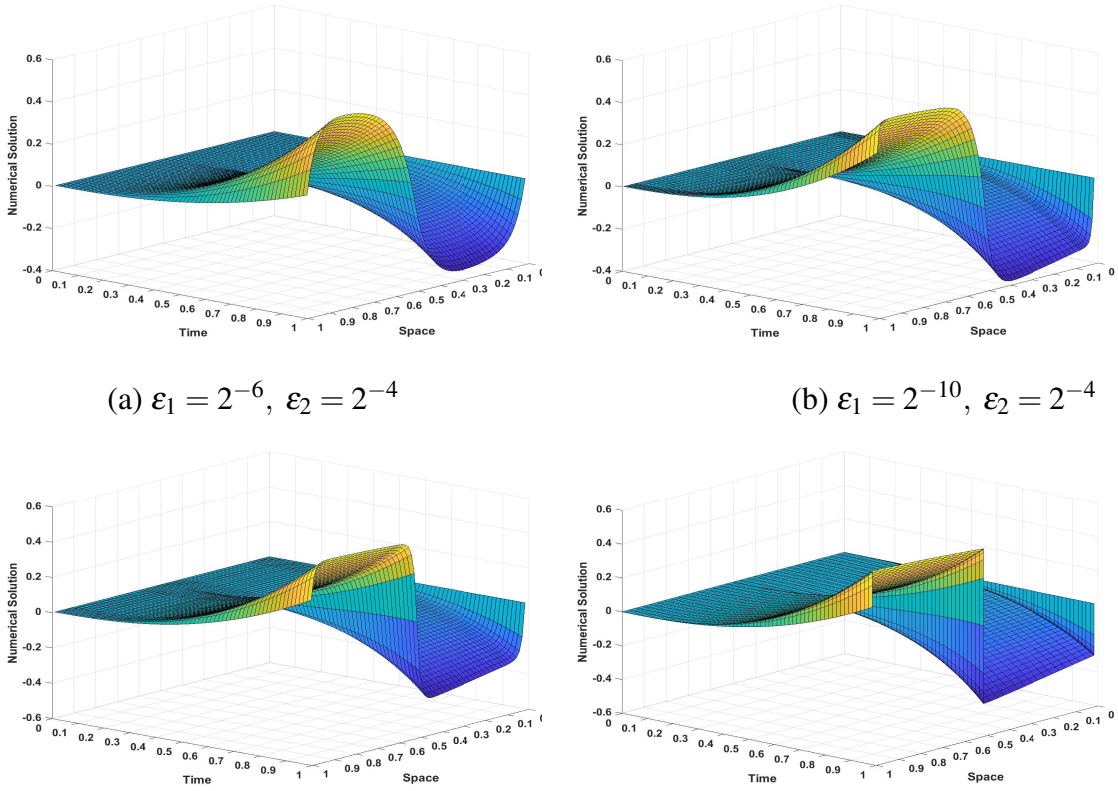

(a) $\varepsilon_1 = 2^{-6},\ \varepsilon_2 = 2^{-4}$ (b) $\varepsilon_1 = 2^{-10},\ \varepsilon_2 = 2^{-4}$

(c) $\varepsilon_1 = 2^{-10},\ \varepsilon_2 = 2^{-20}$ (d) $\varepsilon_1 = 2^{-24},\ \varepsilon_2 = 2^{-32}$

Figure 7.4: Numerical solution profiles for Example 7.5.2.

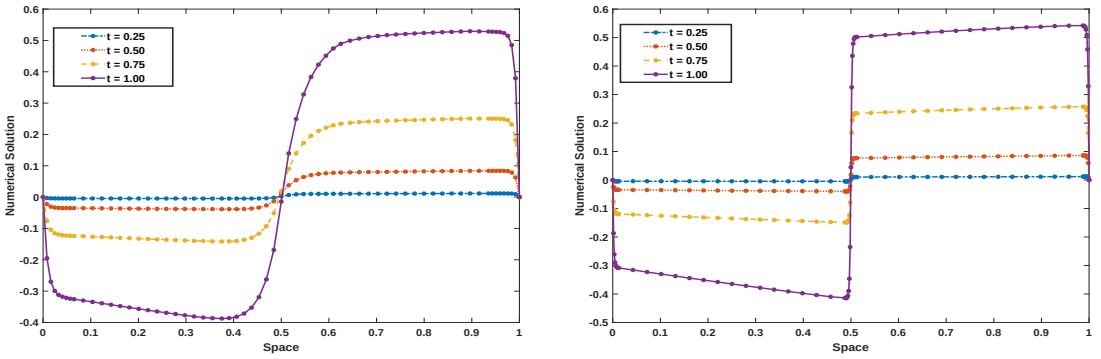

(a) $\varepsilon_1 = 2^{-10},\ \varepsilon_2 = 2^{-4}$ (b) $\varepsilon_1 = 2^{-16},\ \varepsilon_2 = 2^{-24}$

Figure 7.5: Numerical solution profiles for Example 7.5.2.

It is observed from the tables, for fixed $N, \Delta t$, the maximum pointwise error in both cases is fixed after a certain small ε_1 (or ε_2). This confirms the independence of

the method on $\varepsilon_1, \varepsilon_2$. Also, the results presented in the tables confirm the theoretical error estimates obtained in Theorem 7.4.1. All the results presented in the tables are obtained by taking $\Delta t = 1/N$. The physical phenomenon of the solutions for different values of $\varepsilon_1, \varepsilon_2$ is presented via surface plots (refer Figs. 7.1 and 7.4). These graphs clearly indicate that for small perturbation parameters close to zero, the solution of the test problems exhibit parabolic boundary layers at both lateral surfaces, and an interior layer near the point of discontinuity. It can also be observed that the layer width continuously depends on $\varepsilon_1, \varepsilon_2$. The effect of $\varepsilon_1, \varepsilon_2$ for a particular time step on the solution can also be observed from the graphs for different time levels (refer Figs. 7.2 and 7.5).

O'Riordan and Shishkin [134] observed numerically that the discontinuity in the convection-coefficient can lead to only the interior layer when the source function is continuous. Also, it can be noticed from Figure 7.3 that, the interior layer may not appear even if the convection-coefficient is discontinuous, only boundary layers appear that corresponds to the smooth source function. These graphs are drawn by replacing the discontinuous source functions in Examples 7.5.1 and 7.5.2 (keeping $a(x,t)$, $b(x,t)$ and the initial data unchanged) by smooth functions $f(x,t) = 2(1+x^2)t$ and $f(x,t) = (\exp(t^2)-1)(1+xt)$, respectively. All the graphs are drawn by taking $N = 64$ and $\Delta t = 1/N$.

7.6 Conclusion

An implicit numerical scheme on a predefined Shishkin mesh is suggested for the solution of two-parameter singularly perturbed parabolic BVPs where the convection term coefficient and source terms have a jump discontinuity in the domain of consideration. The solution of these problems exhibits twin boundary layers and an interior layer, due to which the analysis of these problems is different from the case of smooth data. For both cases through a rigorous convergence analysis, it has been shown that the proposed scheme is parameters uniform with second-order accuracy in time and almost first-order accuracy in space. Very high gradients near the boundaries Υ_l, Υ_r, and the point of discontinuity e can be observed for small $\varepsilon_1, \varepsilon_2$ (refer Figs. 7.1-7.4). It can also be observed from Figure 7.3 that the interior layer near e may not occur for smooth source term.